Genetic-algorithm-based Design of Large-mode-area All-solid Anti-resonant Fiber with Normal Dispersion and Single-mode Operation in the 2 μm Wavelength Region

Xiaowen Hu, Stefan Gausmann, Md Selim Habib, *Senior Member, IEEE,* Md Abu Sufian, and Axel Schülzgen, *Fellow, OSA*

***Abstract*—Recent years have witnessed much progress in the development of fiber lasers in the 2 μm region. Yet, to date, their power levels are limited by modulation instability and soliton formation attributed to the strong anomalous dispersions of fused silica in this wavelength region. Further power scaling requires a novel design of an all-solid silica active fiber that features normal dispersion by compensating the material dispersion with the waveguide dispersion. At the same time, a large mode area, low losses, single mode operation and robustness need to be maintained. In this paper, we propose an all-solid anti-resonant fiber (AS-ARF) design that meets these demands. We demonstrate that normal dispersion can be achieved in AS-ARFs at 2 μm by exploiting the Kramers-Kronig relation. To balance the desired dispersion with the other performance parameters, we optimize the design of the AS-ARFs using a genetic algorithm. The optimized AS-ARF has a mode field area of 1170 μm^2 and normal dispersion over the spectrum from 1.96 μm to 2.04 μm. Within this spectrum, the maximum confinement loss (CL) of the fundamental mode (FM) is 16 dB/km and the minimum CL of the higher order modes (HOMs) is over 100 dB/km. The HOMs can be easily coupled out by bending the fiber while the FM stays in the core. For example, the CLs are over 2×10^4 dB/km for the HOMs and below 200 dB/km for the FM at 2 μm at a bending radius of 20 cm. Moreover, the properties of the proposed AS-ARF remain favorable even under large geometric variations, showing good tolerance to manufacturing errors. We expect the proposed AS-ARF to further stimulate the development of high-power fiber lasers in the 2 μm region.**

***Index Terms*— Fiber laser, anti-resonant fiber, optical fiber design, genetic algorithm.**

Manuscript received October 19, 2022. This work was supported by the Air Force Research Laboratory under Grants FA8651-18-2-0019 and FA9451-20-C-0015. The first two authors contributed equally to this work.

Xiaowen Hu, Stefan Gausmann, Md Abu Sufian, and Axel Schülzgen are with the University of Central Florida, Orlando, FL 32816 USA (e-mail: steven.hu@knights.ucf.edu; stefan.gausmann@knights.ucf.edu; sufian@knights.ucf.edu; axel@creol.ucf.edu).

Md Selim Habib is with Florida Polytechnic University, Lakeland, FL 33805 USA (email: mhabib@floridapoly.edu).

I. Introduction

FIBER lasers in the 2 μm wavelength region have attracted much attention due to their compactness and wide applications, such as micro-machining [1], light detection and ranging (LIDAR) [2], spectroscopy [3] and telecommunication [4]. Over the past decade, much effort has been devoted to scaling the pulse energy of 2 μm fiber laser systems [5]. It has been shown both theoretically [6-8] and experimentally [9-12], that self-similar pulses or dissipative solitons formed in normal dispersion laser cavities can have much higher pulse energies and peak powers than their counterparts generated in cavities with anomalous dispersion or near zero dispersion [13-19]. Therefore, it is desirable to operate with active fibers that feature normal dispersion at the laser wavelength. Unfortunately, the group velocity dispersions (GVDs) of active fibers in the 2 μm region are dominated by the strong anomalous dispersion of fused silica of ~47 ps/(nm·km). To shift the zero-dispersion wavelength towards longer wavelengths, the anomalous material dispersion has to be compensated by the waveguide dispersion. This can be realized, for example, in a small-core fiber with a W-type index profile [20]. However, high nonlinearity in such small core fibers limits the pulse energy. Increasing the core size for this waveguide design would not only result in multimode operation and a degradation of beam quality but also weaken the waveguide dispersion. A large mode area (LMA) normal dispersive fiber at 2 μm has been proposed by adding a ring of high-index rods in the cladding [21]. However, the proposed fiber struggles to keep single mode operation. Photonic crystal fibers (PCFs) can achieve LMAs with single-mode operation and normal dispersion at 2 μm [22], thanks to the air-hole structures in the cladding. Nevertheless, splicing PCFs to all-glass fibers to form all-fiber laser cavities remains a challenge. Therefore, power scaling of 2 μm fiber lasers calls for novel designs of LMA all-glass fibers with solid single-mode operation and normal dispersion.

To tackle this problem, we adopt the anti-resonant approach that has been widely used in hollow-core fibers [23-25]. Light guidance in such a structure is provided through the inhibited

coupling between the light in the core and the light in the cladding capillary rings [26]. Hollow-core anti-resonant fibers (HC-ARFs) have many favorable properties such as LMAs and low-loss single-mode operation over wide bandwidths. The possibility of dispersion design while maintaining low losses has been demonstrated for HC-ARFs [27]. Recent work has also shown that such approaches can be transferred to all-solid anti-resonant fibers (AS-ARFs) [28, 29]. Moreover, the light guidance can benefit from additional nested capillary rings [30-33], which introduce another degree of freedom in the AS-ARF design.

Since the AS-ARF design problem has a huge parameter space and multiple objective functions, it is not feasible to do a simple parameter sweep. Genetic algorithms (GAs) have been successfully applied to such multi-parameter problems [34]. Inspired by natural evolution, GAs optimize the design parameters by passing the "genes" of good designs to future generations, while introducing randomness through mutations. In this paper, we utilize a GA to search for the optimal design of AS-ARFs for active all-glass fibers in the 2 μm wavelength region. We develop a customized fitness function to evaluate designs, in terms of dispersion, loss, single-mode operation and robustness against bending. By evolving the fiber designs according to their fitness values, we are able to find an AS-ARF design that simultaneously features all desired properties with a mode field area (MFA) of 1170 μm^2, small normal dispersion over the wavelength span from 1.96 μm to 2.04 μm, low confinement loss (CL) of the fundamental mode (FM) of 16 dB/km, high CL of the higher order modes (HOMs) of 108 dB/km which can be significantly further increased by bending, and still acceptable CL of the FM at 2 μm for bending radii down to 20 cm. In addition, we have demonstrated the robustness of our proposed AS-ARF design to geometric variations by a tolerance analysis.

II. Principle

The top left figure in Fig. 1 (a) illustrates the geometrical parameters of the cross-section of the AS-ARF that need to be optimized. For simplicity, only a single ring structure in the cladding is shown. The AS-ARF has a core with radius R_c, in which an area with radius R_{doped} is doped. The ring structure consists of two capillary rings with radii R_1 and R_2, and the same capillary thickness t. The capillary rings are concentric, to avoid the detrimental effects of the touching points between the inner rings and the outer rings that appear in nested HC-ARFs. The eight design parameters of the AS-ARF and their corresponding ranges are listed in the table in Fig. 1 (a). The number of the ring structures in the cladding N can either be 5, 6, 7 or 8. To ensure a LMA, the core radius R_c has a minimum value of 20 μm and can be increased up to 35.5 μm with a step of 0.5 μm. The ratio m of R_{doped}/R_c can be varied between 0.5 and 1. The dopant in the core is assumed to be thulium. The refractive index difference $\Delta n_{doped\ core}$ between the doped core $n_{doped\ core}(\lambda)$ and the fused silica $n_{silica}(\lambda)$ takes values from -0.001 to 0.0025 with an increment of 0.0005. The refractive index of fused silica $n_{silica}(\lambda)$ at wavelength λ is calculated by the Sellmeier equation [35, 36]. The capillary rings are assumed to be doped with germanium to achieve a refractive index difference of Δn_{ring}, which can be varied from 0.015 to 0.05 with a step of 0.005. The capillary thickness t is related to the normalized frequency F at 2 μm through the equation given in the table. According to the Kramers-Kronig relations [37], operating at smaller frequencies near the resonance frequencies can lead to a huge drop in dispersions. Moreover, the anti-resonant reflecting optical waveguide (ARROW) model [38] states that the resonance frequencies occur when F = 1, 2, 3, etc., whereas numerical simulations show that the actual resonance frequencies in ARFs are slightly larger [39, 40]. Therefore, we vary F between 0.95 and 1.1. Once an F is chosen, the capillary thickness t can be readily calculated. The ratio p between R_1 and R_c has a minimum value of $4t/R_c$. Its maximum value can be derived from the geometry. The ratio q between R_2 and R_1 take values from $2t/R_1$ to $1 - 1.5t/R_1$. Each design parameter is converted to a binary string of "genes" with an assigned number of bits (see Supplementary Materials for details). Finally, we combine all the binary strings into a "chromosome" (Fig. 1 (a) top right). In this way, any AS-ARF can be encoded to or decoded from its chromosome.

We create an initial population of 50 individual AS-ARF designs by randomly generating chromosomes (Fig. 1 (b)). To evaluate the "fitness" of the individuals in terms of dispersions, CLs, single-mode operation and robustness, we perform mode analyses over a wavelength span from 1.95 μm to 2.05 μm with a step of 0.01 μm using COMSOL Multiphysics with MATLAB. We define a multi-objective fitness function to calculate the fitness value of each individual:

$$\begin{aligned} & f\left(D(\lambda), CL_{FM}(\lambda), CL_{HOM}(\lambda), CL_{bend}(2\mu m)\right) \\ & = \sigma\left(-\frac{\max\left(D(\lambda)\right)}{10\left[ps/nm\cdot km\right]}\right) \\ & -\sigma\left(\frac{\max\left(CL_{FM}(\lambda)\right)}{10\left[dB/km\right]}-4\right) \\ & +\sigma\left(\frac{\min\left(CL_{HOM}(\lambda)\right)}{30\left[dB/km\right]}\right) \\ & -\frac{1}{20}\sigma\left(\frac{CL_{bend}(2\mu m)}{100\left[dB/km\right]}-4\right) \end{aligned} \quad (1)$$

$D(\lambda)$ is the set of dispersion values over the evaluated spectral range, excluding the first and last wavelengths (see Supplementary Materials). $CL_{FM}(\lambda)$ and $CL_{HOM}(\lambda)$ are the set of CLs of the FMs and the set of the lowest CL of the HOMs at each wavelength, respectively. $CL_{bend}(2\mu m)$ is the CL of the FM at 2 μm when the fiber is bent with a bending radius of 20 cm towards the gap between two ring structures (Supplementary Materials). $\sigma(\cdot)$ is the sigmoid function written as $\sigma(x) = 1/(1+e^{-x})$. We choose the sigmoid function because its curve suits our purpose well. For example, since a

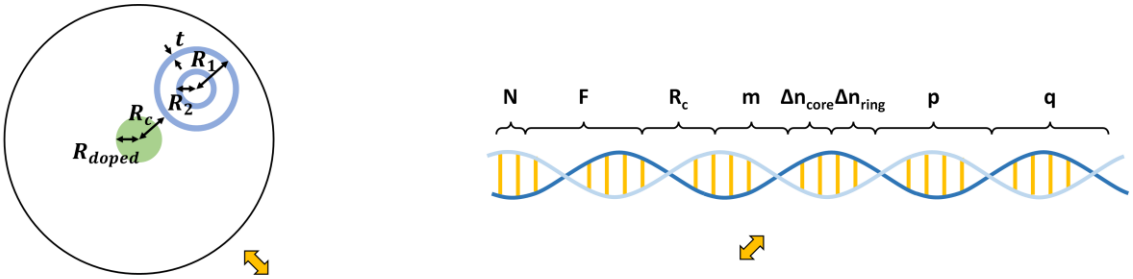

Parameter	Description	Min	Max	Bits
N	Number of ring structures	5	8	2
F	$(2t/\lambda)\sqrt{n_{ring}(\lambda)^2-n_{silica}(\lambda)^2}$ @λ=2μm	0.95	1.1	8
R_c	Core radius (μm)	20	35.5	5
m	R_{doped}/R_c	0.5	1	5
$\Delta n_{doped\ core}$	$n_{doped\ core}(\lambda) - n_{silica}(\lambda)$	-0.001	0.0025	3
Δn_{ring}	$n_{ring}(\lambda) - n_{silica}(\lambda)$	0.015	0.05	3
p	R_1/R_c	$4t/R_c$	$\frac{\sin(\pi/N)}{1-\sin(\pi/N)}$	8
q	R_2/R_1	$2t/R_1$	$1\text{-}1.5t/R_1$	8

(a)

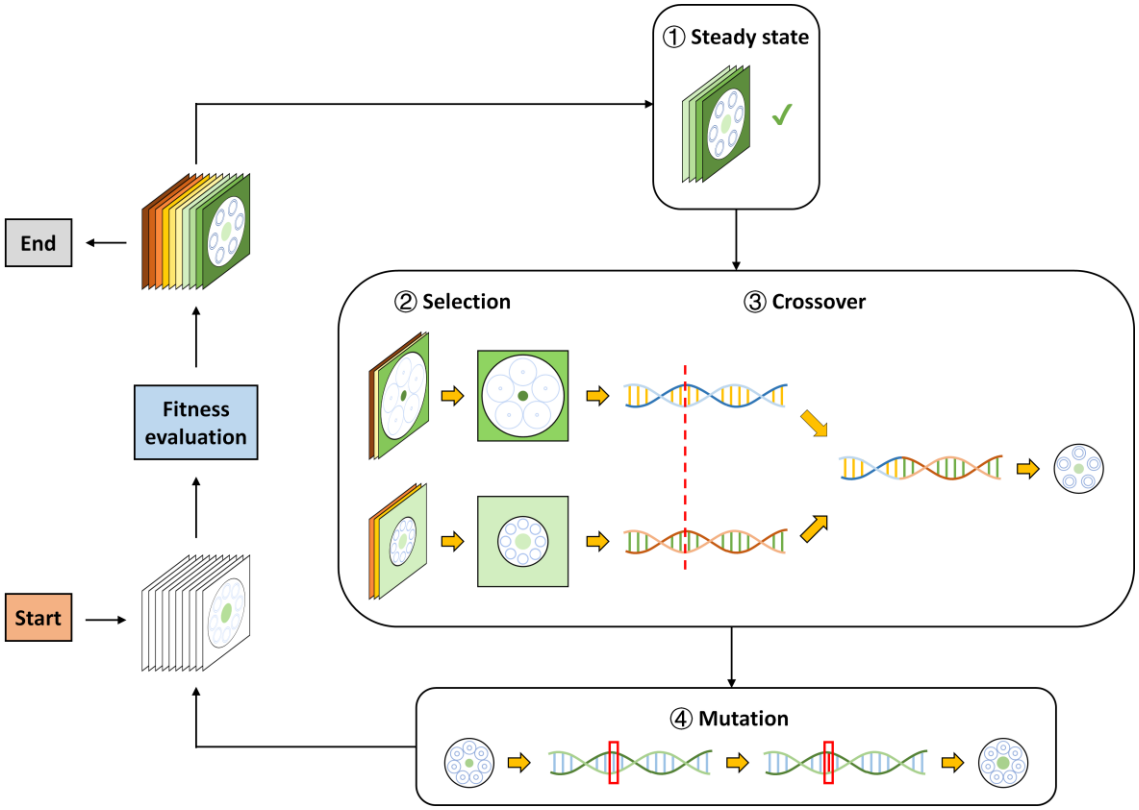

(b)

Fig. 1 (a) Encoding and decoding between the AS-ARF designs and the chromosome representations. Top left: sketch of the cross-section of the AS-ARF to be optimized indicating the geometrical parameters. For simplicity, only one ring structure is shown. Green and blue areas are the doped part of the core and the concentric cladding rings, respectively. Middle: The design parameters, their descriptions and ranges. A number of bits is assigned to each design parameter which create a binary string. Top right: the chromosome of an AS-ARF. It is constructed by appending all the binary strings of the design parameters. (b) Schematic diagram of our GA to optimize the AS-ARF. In each iteration, the fitness of the individuals in the population is evaluated. The new population are produced through several steps, in which the individuals with higher fitness scores have higher chances of passing their genes.

$\max\left(CL_{FM}(\lambda)\right)$ of ~10 dB/km is acceptable for an active fiber at 2 μm, searching for individuals with unnecessarily low CLs should not result in a large gain of the fitness value. On the other hand, the sigmoid function increases rapidly to penalize the GA for generating individuals with $\max\left(CL_{FM}(\lambda)\right)$ beyond 10 dB/km. With even larger $\max\left(CL_{FM}(\lambda)\right)$, the sigmoid function saturates at 1 and prevents the GA from focusing solely on this factor. Therefore, $\left(\frac{\max\left(CL_{FM}(\lambda)\right)}{10[dB/km]}-4\right)$ is chosen as the argument of the sigmoid function, so that $\max\left(CL_{FM}(\lambda)\right)=10[dB/km]$ to $100[dB/km]$ corresponds to the range of most significant increases. We note that the fitness function needs to be and has been carefully tuned to balance the trade-off among the multiple objectives.

After the fitness evaluation, the population goes through several steps to produce the next generation (Fig. 1 (b)). First, the fittest 20% of individuals are immediately kept as the steady state. Next, we perform tournament selections and crossovers on the whole population to create new "children". For each child, we randomly choose 5 individuals and select the fittest one as one parent. Then we repeat the procedure to select the other nonidentical parent. To produce the chromosome of the child, we choose a crossover point at random and exchange the genes of the two parent chromosomes up to the crossover point. New children are generated until the missing 80% of the next population generation is created. Note that a new child is abandoned if the same chromosome has already been included in the population. Finally, we mutate 5% of the total genes in the new population, excluding the top 2 individuals from the previous population, by flipping the binary bits. We conduct mutation until there are no identical chromosomes in the offspring. The GA is run for 100 iterations. The whole process takes ~7 days on a desktop with a 16-core CPU and 128 G memory.

III. Results

Fig. 2 shows the average values of the top 20% fittest individuals in each iteration. As can be seen, the average fitness score $\overline{\text{Fitness}}$ (the black curve) increases rapidly over the first several iterations and then reaches a plateau. After evolving for many generations, a much fitter individual is produced at the 36th iteration. Its genes are passed to future populations, which significantly improves their fitness. Similar behavior can be observed in $\overline{\max\left(D(\lambda)\right)}$ (the red curve), which decreases greatly after the 36th iteration and eventually reaches normal dispersion. Moreover, we also notice the trade-off among the multiple objectives. $\overline{\max\left(CL_{FM}(\lambda)\right)}$ (the blue curve), $\overline{\min\left(CL_{HOM}(\lambda)\right)}$ (the yellow curve) and $\overline{CL_{bend}(2\mu m)}$ (the green curve) all move away from their own targets in the early stage, when the GA manages to trade them off for larger overall fitness scores.

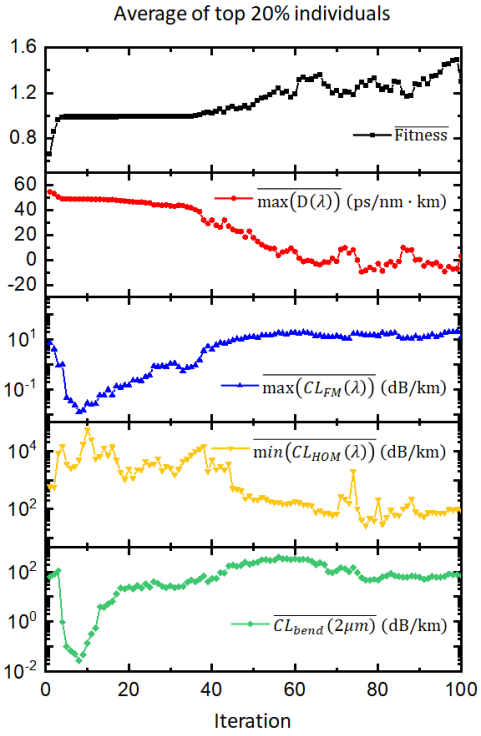

Fig. 2 The averaged values of the top 20% individuals in the population as a function of iteration.

The optimized AS-ARF after 100 iterations has a fitness score of 1.5298. Its design parameters are N = 5, F = 1.01328125, R_c = 20 μm, m = 0.984375, $\Delta n_{\text{doped core}}$ = 0.001, Δn_{ring} = 0.045, p = 1.087259912379027 and q = 0.800768685699695, which translate to $R_{\text{doped}} \approx 19.69$ μm, $R_1 \approx 21.75$ μm, $R_2 \approx 17.41$ μm, and $t \approx 2.795$ μm in the optimized design (Fig. 3 (a)). The optimized AS-ARF features a large FM with a MFA of 1170 μm^2 (see Supplementary Materials). The FM is in the normal dispersion regime over the whole target spectrum from 1.96 μm to 2.04 μm (Fig. 3 (b) top), with low CLs (maximum CL = 16 dB/km at 1.96 μm) (Fig. 3 (b) bottom, red line). Moreover, the CL_{HOM} stays relatively high in the wavelength range, with a minimum value larger than 100 dB/km (Fig. 3 (b) bottom, the blue line). The CL_{HOM} can be further increased if the fiber is bent, allowing strict single-mode operation. For example, the CL_{HOM} is more than 2×10^4 dB/km at 2 μm when the bending radius is 20 cm. In the meanwhile, the FM exhibits robustness to fiber deformations. In Fig. 3 (c), we plot the CL_{FM} at 2 μm when the AS-ARF is bent towards the gap between the ring structure (the yellow line) or bent towards the ring structure (the green line). The bending radius is decreased from 100 cm to 5 cm in -5 cm steps. The CL_{FM} remains relatively small even when the AS-ARF is substantially bent. At a bending radius of 20 cm, CL_{FM} is less than 200 dB/km.

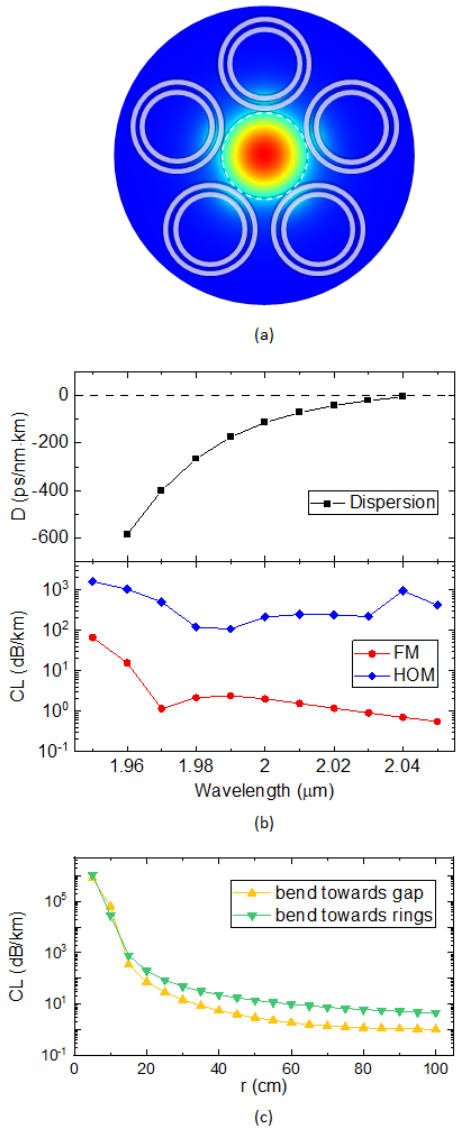

Fig. 3 (a) The cross-section of the optimized AS-ARF by GA, together with the mode profile of the FM. (b) Top: the dispersion of the FM from 1.96 to 2.04 μm. Bottom: The CLs of the FM (the red lines) and HOMs (the blue lines) from 1.95 to 2.05 μm. (c) The CLs of the FM as a function of the bending radius when the AS-ARF is bent towards the gap between ring structures (the yellow lines) or towards the ring structure (green lines).

We further investigate the tolerance of the AS-ARF design to fabrication errors, when the geometric parameters R_1 and $d = R_1 - t - R_2$ deviate from the values given by the GA, i.e., R_1 = 21.75 μm and d = 1.545 μm (Fig. 4 (a)). We vary R_1 from 20 μm to 24 μm with a step of 0.5 μm, and d from 0.8 μm to 2 μm with a step of 0.1 μm. Fig. 4 (b)-(f) plot the overall fitness scores, $\max\left(D(\lambda)\right)$, $\max\left(CL_{FM}(\lambda)\right)$, $\min\left(CL_{HOM}(\lambda)\right)$ and $CL_{bend}(2\mu m)$ of the designs with different combinations of the geometric parameters, respectively. Several observations can be made. First and foremost, we can see high fitness scores in a large region of geometric parameters (the red area in Fig. 4 (b)), which indicates the good tolerance of the AS-ARF design to geometric variations. Secondly, the trade-off between multiple objectives can again be observed. As each individual objective requires the geometric parameters to go in a certain direction, the overall fitness has a hill shape with an optimum peak value (the black triangle) that represents the best balance among all the objectives. Moreover, we notice that the geometric values given by the GA (the white square) deviate a little from the actual optimum values (the black triangle), i.e., R_1 = 21.75 μm and d = 1.2 μm. We expect the GA to converge to these optimum values if we run more iterations. Nevertheless, the GA manages to locate the hill in the fitness mapping and find designs with high fitness scores after 100 iterations.

IV. Discussion and Conclusion

By applying a GA, we found an AS-ARF design that features highly desired properties for active fibers operating around 2 μm. This AS-ARF can be fabricated using fairly conventional fiber drawing techniques, and shows robust performance regarding fabrication errors. The excellent properties of the proposed AS-ARF can be attributed to a superposition of resonances in the cladding. This becomes clear considering Fig. 5 where we compare CL_{FM}, dispersion and CL_{HOM} of the proposed AS-ARF with nested rings (the black lines) and the one with the same design parameters but only a single ring in the cladding structure (the red lines). It can be seen in Fig. 5 (top), that the single ring structure has one major high loss peak as predicted by the ARROW model [38], whereas the nested ring structure has an additional loss peak. The FM can be coupled to the additional cladding modes introduced by the nested ring structure, which broadens the high loss regime (compare the red area with the blue area). Since the proposed AS-ARF operates near the high loss region (the yellow box), the superposition of the resonances results in a greatly decreased dispersion (Fig. 5 middle), thanks to the Kramers-Kronig relations [37]. On the other hand, although the nested ring structure generally reduces CL_{FM} and CL_{HOM} in the low loss region (beyond 2.1 μm in Fig. 5 top and bottom), the losses are higher than the single ring structure in the operating wavelength range close to the high loss region (the yellow box), in analogy to nested HC-ARFs [31]. Therefore, great care must be taken to design a nested ring structure with desirable properties in the operating wavelength range. However, due to the complicated structure, there is no analytical function that fully describes the relationship between the design parameters and the optical properties. To date, the design process is mainly carried out through long parameter sweeps. In contrast, we show that the GA offers an effective and systematic way to find designs that can balance multiple objectives without tedious, time-consuming parameter sweeps.

Fabrication of the proposed AS-ARF is feasible, as described, e.g., in Ref. [29], thanks to the advanced manufacturing technology of all-solid fibers. First, the rods of the thulium-doped active core and the germanium-doped ring structures are to be prepared. Both can be achieved by modified chemical vapor deposition (MCVD). The fabrication of the latter can be similar to that of Bragg fibers with radially modulated refractive index profiles [41, 42]. Alternatively,

reactive powder sinter technology can be utilized to enable a more uniform refractive index profile with improved accuracy [43, 44]. Secondly, holes are to be drilled in the active core rod using precise drilling technology, which has been widely used in fabricating polarization maintaining fibers [45]. Next, the rods of ring structure can be inserted into the active core rod to complete the preform. Finally, the preform can be drawn to produce the proposed AS-ARF.

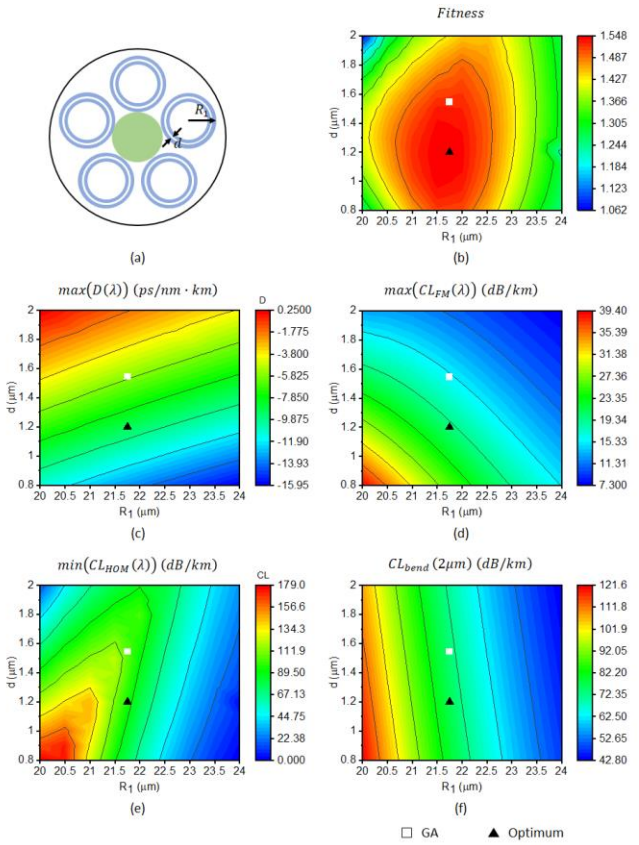

Fig. 4 Test of the tolerance of the AS-ARF design to changes of the geometric parameters that might occur due to fabrication errors. (a) R_1 and $d = R_1 - t - R_2$ are varied around the values given by the GA. (b-f) The overall fitness scores, $\max(D(\lambda))$, $\max(CL_{FM}(\lambda))$, $\min(CL_{HOM}(\lambda))$ and $CL_{bend}(2\mu m)$ of the designs with different combinations of the geometric parameters, respectively. White squares: the geometric parameters given by the GA. Black triangles: the actual optimum geometric parameters in terms of the fitness score. The GA is expected to converge to the black triangles with more iterations.

Future studies can be made in several directions. First, although the requirement of LMAs has been included in the ranges of the design parameters R_c and m, it is not reflected in the fitness function. Given the current fitness function, the GA converges quickly to the smallest possible R_c of 20 µm. Future work can be done to add an extra term in the fitness function in order to drive the GA to find designs with larger LMAs. Secondly, the current design adopts the same design principle of the nested HC-ARFs, where the inner and outer capillary rings have the same thicknesses [30-33]. In nested HC-ARFs, the identical ring thickness is to prevent the introduction of additional high loss regions. However, this is no longer required for the current purpose. As shown in Fig. 5, additional high loss peaks can decrease the dispersion at 2 µm without sacrificing much of the loss performance. Future work can be done to investigate the possibility of using different thicknesses for the inner and outer capillary rings.

In conclusion, we propose an AS-ARF design that fulfills the requirements of an active fiber for further power scaling of lasers and amplifiers in the 2 µm region, e.g., small normal dispersion over a wide wavelength range, LMA, low FM loss, single mode operation, and robustness. We show that this is achieved by operating near cladding resonances where the dispersions can be greatly reduced without sacrificing much of other desirable properties. By utilizing a GA, we successfully find a combination of the design parameters that can balance multiple objectives. With these great results, we expect the implementation of the proposed AS-ARF in the next-generation high power fiber lasers in the 2 µm region.

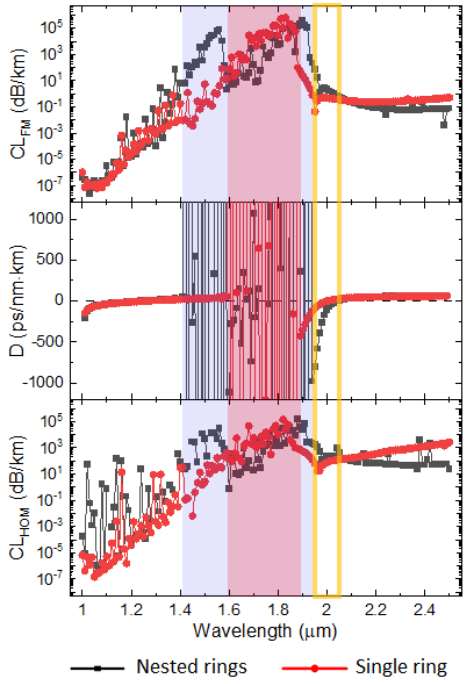

Fig. 5 The comparisons of (top) CL_{FM}, (middle) dispersion, and (bottom) CL_{HOM} between the proposed AS-ARF with nested rings (the black lines) and the AS-ARF with the same design parameters but has single ring in the ring structure (the red lines). The blue area and the red area demonstrate the high loss region of these two designs, respectively. The yellow box marks the operating wavelength range around 2 µm.

REFERENCES

[1] S. Singh and G. L. Samuel, "Laser Micromachining of Semiconductor Materials," in *Application of Lasers in Manufacturing* (2019), pp. 111-141.

[2] F. Gibert, D. Edouart, C. Cénac, F. Le Mounier, and A. Dumas, "2-µm Ho emitter-based coherent DIAL for CO_2 profiling in the atmosphere," Optics Letters **40** (2015).

[3] N. Picqué and T. W. Hänsch, "Frequency comb spectroscopy," Nature Photonics **13**, 146-157 (2019).

[4] R. Soref, "Enabling 2 µm communications," Nature Photonics **9**, 358-359 (2015).

[5] D. C. Kirsch, S. Chen, R. Sidharthan, Y. Chen, S. Yoo, and M. Chernysheva, "Short-wave IR ultrafast fiber

laser systems: Current challenges and prospective applications," Journal of Applied Physics **128** (2020).

[6] H. A. Haus, J. G. Fujimoto, and E. P. Ippen, "Structures for additive pulse mode locking," Journal of the Optical Society of America B **8** (1991).

[7] F. Ö. Ilday, J. R. Buckley, W. G. Clark, and F. W. Wise, "Self-Similar Evolution of Parabolic Pulses in a Laser," Physical Review Letters **92** (2004).

[8] W. H. Renninger, A. Chong, and F. W. Wise, "Dissipative solitons in normal-dispersion fiber lasers," Physical Review A **77** (2008).

[9] A. Chong, J. Buckley, W. Renninger, and F. Wise, "All-normal-dispersion femtosecond fiber laser," Optics Express **14** (2006).

[10] F. W. Wise, A. Chong, and W. H. Renninger, "High-energy femtosecond fiber lasers based on pulse propagation at normal dispersion," Laser & Photonics Review **2**, 58-73 (2008).

[11] K. Kieu, W. H. Renninger, A. Chong, and F. W. Wise, "Sub-100 fs pulses at watt-level powers from a dissipative-soliton fiber laser," Optics Letters **34** (2009).

[12] A. Chong, L. G. Wright, and F. W. Wise, "Ultrafast fiber lasers based on self-similar pulse evolution: a review of current progress," Reports on Progress in Physics **78** (2015).

[13] L. E. Nelson, E. P. Ippen, and H. A. Haus, "Broadly tunable sub-500 fs pulses from an additive-pulse mode-locked thulium-doped fiber ring laser," Applied Physics Letters **67**, 19-21 (1995).

[14] D. Anderson, M. Desaix, M. Lisak, and M. L. Quiroga–Teixeiro, "Wave breaking in nonlinear-optical fibers," Journal of the Optical Society of America B **9** (1992).

[15] G. P. Agrawal, *Applications of Nonlinear Fiber Optics*, Academic Press (2008).

[16] A. Hasegawa, M. Matsumoto, *Optical Solitons in Fibers*, Springer Series in Photonics (2003).

[17] H. A. Haus, K. Tamura, L. E. Nelson, and E. P. Ippen, "Stretched-pulse additive pulse mode-locking in fiber ring lasers: theory and experiment," IEEE Journal of Quantum Electronics **31**, 591-598 (1995).

[18] B. A. Malomed, *Soliton Management in Periodic Systems*, Springer, (2006).

[19] Y. Tang, A. Chong, and F. W. Wise, "Generation of 8 nJ pulses from a normal-dispersion thulium fiber laser," Optics Letters **40** (2015).

[20] Y. Chen, S. Yoo, S. Chen, R. Sidharthan, C. J. Cheng, K. Liu, S. Rao, O. Bang, Q. Wang, and D. Y. Tang, "High Energy Ultrafast Laser at 2 μm Using Dispersion Engineered Thulium-Doped Fiber," IEEE Photonics Journal **11**, 1-12 (2019).

[21] C. Baskiotis, A. M. Heidt, S. Alam, and D. J. Richardson, "LMA effectively single-mode thulium doped fibre with normal dispersion at wavelengths around 2 μm," in 2013 Conference on Lasers & Electro-Optics Europe & International Quantum Electronics Conference CLEO EUROPE/IQEC, (2013), pp. 1-1.

[22] N. Modsching, P. Kadwani, R. A. Sims, L. Leick, J. Broeng, L. Shah, and M. Richardson, "Lasing in thulium-doped polarizing photonic crystal fiber," Optics Letters **36** (2011).

[23] A. D. Pryamikov, A. S. Biriukov, A. F. Kosolapov, V. G. Plotnichenko, S. L. Semjonov, and E. M. Dianov, "Demonstration of a waveguide regime for a silica hollow-core microstructured optical fiber with a negative curvature of the core boundary in the spectral region > 3.5 μm," Optics Express **19** (2011).

[24] F. Yu and J. C. Knight, "Negative Curvature Hollow-Core Optical Fiber," IEEE Journal of Selected Topics in Quantum Electronics **22**, 146-155 (2016).

[25] C. Wei, R. Joseph Weiblen, C. R. Menyuk, and J. Hu, "Negative curvature fibers," Advances in Optics and Photonics **9** (2017).

[26] B. Debord, A. Amsanpally, M. Chafer, A. Baz, M. Maurel, J. M. Blondy, E. Hugonnot, F. Scol, L. Vincetti, F. Gérôme, and F. Benabid, "Ultralow transmission loss in inhibited-coupling guiding hollow fibers," Optica **4** (2017).

[27] A. N. Kolyadin, G. K. Alagashev, A. D. Pryamikov, L. Mouradian, A. Zeytunyan, H. Toneyan, A. F. Kosolapov, and I. A. Bufetov, "Negative Curvature Hollow-core Fibers: Dispersion Properties and Femtosecond Pulse Delivery," Physics Procedia **73**, 59-66 (2015).

[28] X. Zhang, S. Gao, Y. Wang, W. Ding, and P. Wang, "Design of large mode area all-solid anti-resonant fiber for high-power lasers," High Power Laser Science and Engineering **9** (2021).

[29] Z. Xing, X. Wang, S. Lou, Z. Tang, H. Jia, S. Gu, and J. Han, "Large-mode-area all-solid anti-resonant fiber with single-mode operation for high-power fiber lasers," Optics Letters **46** (2021).

[30] W. Belardi and J. C. Knight, "Hollow antiresonant fibers with reduced attenuation," Optics Letters **39** (2014).

[31] F. Poletti, "Nested antiresonant nodeless hollow core fiber," Optics Express **22** (2014).

[32] T. D. Bradley, J. R. Hayes, Y. Chen, G. T. Jasion, S. R. Sandoghchi, R. Slavik, E. N. Fokoua, S. Bawn, H. Sakr, I. A. Davidson, A. Taranta, J. P. Thomas, M. N. Petrovich, D. J. Richardson, and F. Poletti, "Record Low-Loss 1.3 dB/km Data Transmitting Antiresonant Hollow Core Fibre," in 2018 European Conference on Optical Communication (ECOC), (2018), pp. 1-3.

[33] G. T. Jasion, T. D. Bradley, K. Harrington, H. Sakr, Y. Chen, E. N. Fokoua, I. A. Davidson, A. Taranta, J. R. Hayes, D. J. Richardson, and F. Poletti, "Hollow Core NANF with 0.28 dB/km Attenuation in the C and L Bands," in Optical Fiber Communication Conference Postdeadline Papers, (2020).

[34] S. Katoch, S. S. Chauhan, and V. Kumar, "A review on genetic algorithm: past, present, and future," Multimedia Tools and Applications **80**, 8091-8126 (2020).

[35] Sellmeier, "Zur Erklärung der abnormen Farbenfolge im Spectrum einiger Substanzen," Annalen der Physik und Chemie **219**, 272-282 (1871).

[36] I. H. Malitson, "Interspecimen Comparison of the Refractive Index of Fused Silica" Journal of the Optical Society of America **55** (1965).

[37] R. de L. Kronig, "On the Theory of Dispersion of X-Rays," Journal of the Optical Society of America **12** (1926).
[38] N. M. Litchinitser, A. K. Abeeluck, C. Headley, and B. J. Eggleton, "Antiresonant reflecting photonic crystal optical waveguides," Optics Letters **27** (2002).
[39] L. Vincetti and V. Setti, "Waveguiding mechanism in tube lattice fibers," Optics Express **18** (2010).
[40] L. Vincetti, "Empirical formulas for calculating loss in hollow core tube lattice fibers," Optics Express **24** (2016).
[41] S. Février, P. Viale, Géro, F. me, P. Leproux, P. Roy, J. M. Blondy, B. Dussardier, and G. Monnom, "Very large effective area singlemode photonic bandgap fibre," Electronics Letters **39** (2003).
[42] S. Février, R. Jamier, J. M. Blondy, S. L. Semjonov, M. E. Likhachev, M. M. Bubnov, E. M. Dianov, V. F. Khopin, M. Y. Salganskii, and A. N. Guryanov, "Low-loss singlemode large mode area all-silica photonic bandgap fiber," Optics Express **14** (2006).
[43] K. Schuster, S. Unger, C. Aichele, F. Lindner, S. Grimm, D. Litzkendorf, J. Kobelke, J. Bierlich, K. Wondraczek, and H. Bartelt, "Material and technology trends in fiber optics," Advanced Optical Technologies **3** (2014).
[44] D. Darwich, R. Dauliat, R. Jamier, A. Benoit, J.-L. Auguste, S. Grimm, J. Kobelke, A. Schwuchow, K. Schuster, and P. Roy, "50.4% slope efficiency thulium-doped large-mode-area fiber laser fabricated by powder technology," Optics Letters **41** (2016).
[45] J. Noda, K. Okamoto, and Y. Sasaki, "Polarization-maintaining fibers and their applications," Journal of Lightwave Technology **4**, 1071-1089 (1986).

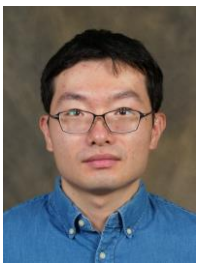

Xiaowen Hu received his Ph.D. degree in Optics and Photonics from CREOL, the College of Optics and Photonics, at University of Central Florida, USA, in 2022. He received his B.S. degree in Optical Science and Technology from Fudan University, China, in 2015. His research interests include microstructured fiber optics, machine learning applications in optical design and optical fiber imaging.

Stefan Gausmann received a B.S. and a M.S. degree in physics from RWTH Aachen University, Aachen, Germany, in 2014 and 2016, respectively. He received a second M.S. degree in 2017 and a PhD degree in 2021 in Optics and Photonics from the University of Central Florida, Orlando, FL, USA. His current research interests include high power CW fiber lasers and nonlinear optics.

Md. Selim Habib (S'13–SM'19) received the B.Sc. and M.Sc. Degrees in Electrical and Electronic Engineering from Rajshahi University of Engineering and Technology, Rajshahi, Bangladesh in 2008 and 2012 respectively. He received the Ph.D. degree in photonics engineering from Technical University of Denmark (DTU) in 2017. After finishing his Ph.D., he joined as a Postdoctoral Researcher in Fibers Sensors and Supercontinuum Group at the Department of Photonics Engineering, DTU. After finishing his Postdoctoral Fellowship at DTU, he worked as a Postdoctoral Research Associate at CREOL, The College of Optics and Photonics, University of Central Florida, USA from September, 2017 to August, 2019. Now he is an Assistant Professor of Electrical and Computer Engineering at Florida Polytechnic University, USA. His research mainly focuses on design, fabrication, and characterization of low loss hollow core fiber in the near-IR to mid-IR, light gas nonlinear interaction in hollow core fibers, supercontinuum generation, and multi-mode nonlinear optics. He has published more than 40 articles in referred journals. Dr. Habib is a Senior Member of Institute of Electrical and Electronics Engineers (IEEE) and Optica, and Executive officer of Optica Fiber modeling and Fabrication group. Dr. Habib is an Associate Editor of IEEE Access, and Feature Editor of Applied Optics (OSA). He received the University Gold Medal Award from Rajshahi University of Engineering and Technology in 2014.

Md. Abu Sufian received his B.S. in Electrical and Electronic Engineering from Khulna University of Engineering and Technology, Khulna, Bangladesh and the M.S. degree in Materials and Devices from Electrical and Computer Engineering department, University of Delaware, Delaware, USA. He is currently working toward the Ph.D. degree in CREOL- The College of Optics and Photonics, University of Central Florida, Florida, USA. His research interests include design, fabrication, and characterization of new generation hollow core fibers, fiber bundles and components for imaging applications, laser systems and fiber optic communications.

Axel Schülzgen received the Ph.D. degree in physics from the Humboldt University of Berlin, Germany. Since 2009, he has been a Professor of Optics and Photonics with the Center for Research and Education in Optics and Lasers, The College of Optics and Photonics, University of Central Florida, Orlando, FL, USA. He also holds an Adjunct Professor position with the College of Optical Sciences, The University of Arizona, Tucson, AZ, USA. His current research interests include optical fiber devices, components, materials, and structures with applications in fiber laser systems, fiber optic sensing and imaging, and optical communications. He is a Fellow of the Optica and the International Society for Optics and Photonics SPIE.